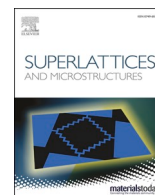




ELSEVIER

Contents lists available at ScienceDirect

Superlattices and Microstructures

journal homepage: www.elsevier.com/locate/superlattices

Microstructure and temperature-dependence of Raman scattering properties of β -(Al_xGa_{1-x})₂O₃ crystals

Xian Chen^{a,c}, Wenlong Niu^a, Lingyu Wan^{a,c,*}, Changtai Xia^b, Huiyuan Cui^b,
Devki N. Talwar^d, Zhe Chuan Feng^{a,c}

^a Center on Nanoenergy Research, Laboratory of Optoelectronic Materials & Detection Technology, Guangxi Key Laboratory for the Relativistic Astrophysics, School of Physical Science & Technology, Guangxi University, Nanning, 530004, China

^b Shanghai Institute of Optics and Fine Mechanics, Chinese Academy of Sciences, 201800, Shanghai, China

^c State Key Laboratory of Luminescence and Applications, Changchun Institute of Optics, Fine Mechanics and Physics, Chinese Academy of Sciences, Changchun, 130033, China

^d Department of Physics, University of North Florida, Jacksonville, FL, 32224, USA

ARTICLE INFO

Keywords:

Ga₂O₃ crystal
Lattice structure
Raman phonon modes
Temperature dependence

ABSTRACT

Bulk crystals of β -Ga₂O₃, (Al_{0.1}Ga_{0.9})₂O₃ and (Al_{0.2}Ga_{0.8})₂O₃ were grown by the optical floating zone and edge-defined film-fed methods. Their microstructure and temperature-dependent phonon characteristics were investigated systematically by using high resolution X-ray diffraction (HR-XRD) and Raman scattering spectroscopy. HR-XRD results revealed a very good crystalline phase for all the samples. As compared to the pure β -Ga₂O₃, the interplanar spacings in (Al_{0.1}Ga_{0.9})₂O₃ and (Al_{0.2}Ga_{0.8})₂O₃ samples are found decreasing with the increase of Al contents – exhibiting distorted lattice structures. Due to the deformations in (Al_xGa_{1-x})₂O₃, the Raman peaks revealed redshifts and linewidth broadening as the Al composition (x) is increased. The lattice distortion mainly affected the Raman modes in the range of less than 600 cm⁻¹ and had a relatively trivial effect on the modes higher than 600 cm⁻¹. With the increase of temperature, the Raman peaks are also redshifted and linewidth broadened. Similar to a pure β -Ga₂O₃, our Raman shifts in the two (Al_xGa_{1-x})₂O₃ crystals revealed quadratic dependence on temperature – showing specific relationships. However, the temperature dependent widening of the Raman active phonons in (Al_xGa_{1-x})₂O₃ exhibited a convoluted behavior different from β -Ga₂O₃. The results are significant for further understanding of (Al_xGa_{1-x})₂O₃ crystals and evaluating its use in device applications.

1. Introduction

β -Ga₂O₃ is a transparent oxide possessing ultra-wide bandgap (E_g, 4.5–4.9 eV), which has attracted extensive research interests in recent years. Compared with other wide-bandgap semiconductors such as SiC and GaN, it has excellent merits of larger band gap, stronger breakdown field, shorter absorption cut-off edge and lower growth cost [1–3]. It is expected to be a preferred material for the next generation devices of high voltage, high power with low loss devices and deep ultraviolet optoelectronic detectors [4].

* Corresponding author. Center on Nanoenergy Research, Laboratory of Optoelectronic Materials & Detection Technology, Guangxi Key Laboratory for the Relativistic Astrophysics, School of Physical Science & Technology, Guangxi University, Nanning, 530004, China.

E-mail address: LYW2017@gxu.edu.cn (L. Wan).

<https://doi.org/10.1016/j.spmi.2020.106469>

Received 27 September 2019; Received in revised form 5 February 2020; Accepted 25 February 2020

Available online 28 February 2020

0749-6036/© 2020 Elsevier Ltd. All rights reserved.

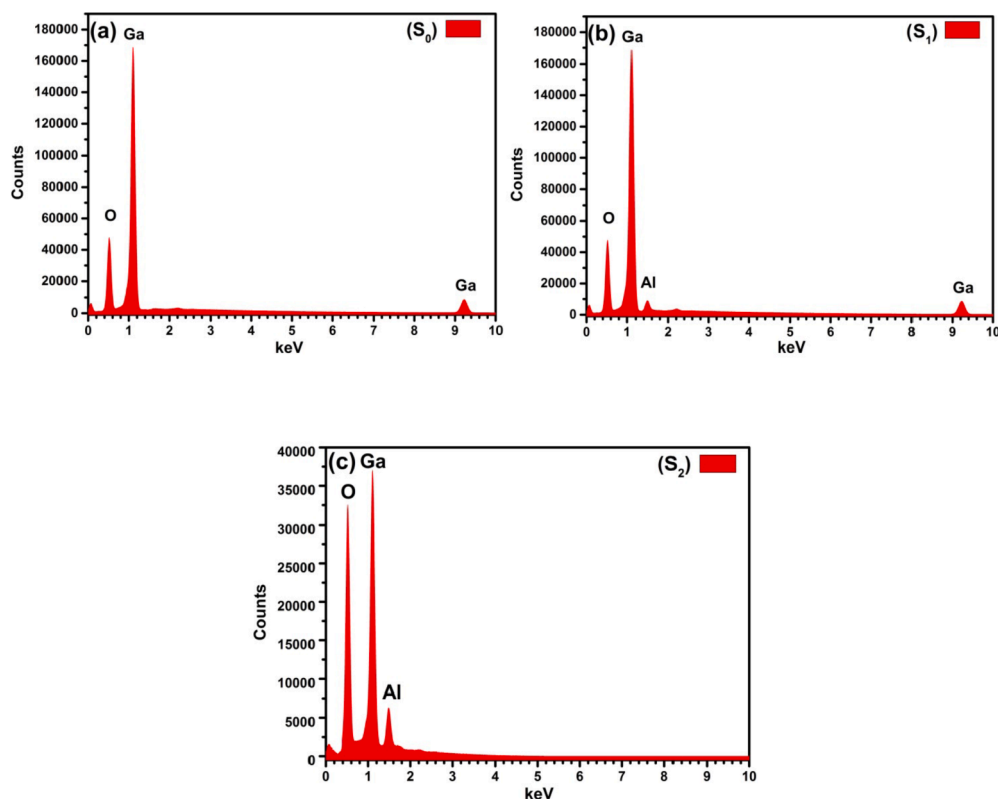


Fig. 1. The measurement results of EDS for S_0 , S_1 , S_2 , respectively.

It is fundamental to explore the materials with flexible and tunable bandgap to improve the functionality of Ga_2O_3 -based devices. In this regard, good candidates with bandgap tunability are $(\text{Al}_x\text{Ga}_{1-x})_2\text{O}_3$ and $(\text{In}_x\text{Ga}_{1-x})_2\text{O}_3$ materials. With the increase of Al or In content (x), the bandgap of $(\text{Al}_x\text{Ga}_{1-x})_2\text{O}_3$ increases [5,6], while in $(\text{In}_x\text{Ga}_{1-x})_2\text{O}_3$ it decreases [7,8]. Because of the absorption cut-off wavelength extended to the vacuum deep ultraviolet region and with a good capability of bandgap adjusting, the $(\text{Al}_x\text{Ga}_{1-x})_2\text{O}_3$ materials have attracted much attention. However, due to the different atomic radius, lattice positions, and the formation of new complexes and defects during the crystal growth process, Al-incorporation not only modifies the bandgap of material, but also changes the crystal structure and physical properties [9,10]. Thus, understanding the influence of different Al content on the structure and intrinsic properties of materials is of great significance for material growth and device applications.

There exist some reports in the literature on $(\text{Al}_x\text{Ga}_{1-x})_2\text{O}_3$ powder samples and thin films. Krueger et al. investigated the structural properties of $(\text{Al}_x\text{Ga}_{1-x})_2\text{O}_3$ ($0 \leq x < 0.8$) powders. It was found that with the increase of Al content, the lattice parameters would shrink and the bandgap enlarged [11]. Escribano et al. studied the $(\text{Al}_x\text{Ga}_{1-x})_2\text{O}_3$ powders prepared by aluminum nitrate and gallium nitrate, and calculated the mutual solubility of Ga and O in oxides [12]. Li et al. researched on the $(\text{Al}_x\text{Ga}_{1-x})_2\text{O}_3$ thin films grown by laser molecular beam epitaxy and considered that Al ions tend to replace the tetrahedral position of Ga. Theoretical calculations showed that $(\text{Al}_x\text{Ga}_{1-x})_2\text{O}_3$ has indirect nature of bandgap with the increase of Al content due to the increase of eigenvalue gap between M point and Γ point in the valence band [13]. Kranert et al. prepared $(\text{Al}_x\text{Ga}_{1-x})_2\text{O}_3$ thin films by using the pulsed laser deposition (PLD) method and reported the lattice parameters and phonon energy properties [14]. Ma et al. studied the effect of intrinsic defects on the electrical and optical properties of Al-doped Ga_2O_3 by first principle calculations [15].

Compared with the powder and thin film materials, bulk $(\text{Al}_x\text{Ga}_{1-x})_2\text{O}_3$ single crystals are difficult to grow and only limited reports exist in the literature [16]. Their crystal structures are more sensitive to the Al content and the growth conditions. However, the crystalline and temperature-dependent properties of different $(\text{Al}_x\text{Ga}_{1-x})_2\text{O}_3$ single crystals are still lacking for a systematic study. In this paper, we investigated bulk $\beta\text{-Ga}_2\text{O}_3$ crystals and alloyed with 10% Al and 20% Al grown by the optical floating zone (OFZ) and edge-defined film-fed (EFG) methods. The effects of Al-alloying on the crystal structure of $(\text{Al}_x\text{Ga}_{1-x})_2\text{O}_3$ has been analyzed by HR-XRD, and the optical phonon modes were studied by temperature-dependent Raman scattering spectroscopy in the range of 80–800 K.

2. Experimental

Bulk $\beta\text{-Ga}_2\text{O}_3$ and $(\text{Al}_x\text{Ga}_{1-x})_2\text{O}_3$ ($x \approx 0.2$) crystals were grown by OFZ, and $(\text{Al}_x\text{Ga}_{1-x})_2\text{O}_3$ ($x \approx 0.1$) crystal was grown by EFG. The three samples were labeled as S_0 ($\beta\text{-Ga}_2\text{O}_3$), S_1 ($\text{Al}_{0.1}\text{Ga}_{0.9}$) $_2\text{O}_3$ and S_2 ($\text{Al}_{0.2}\text{Ga}_{0.8}$) $_2\text{O}_3$, respectively. The Al compositions of $(\text{Al}_x\text{Ga}_{1-x})_2\text{O}_3$ samples are first evaluated through energy-dispersive X-ray spectroscopy (EDS, JXA-8230, Japan Electron Optics Laboratory Co,

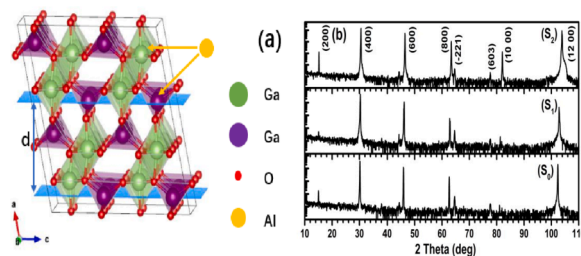


Fig. 2. (a) The scheme of β -Ga₂O₃ crystal structure; (b) HR-XRD 2θ scan of S₀, S₁ and S₂.

Table 1
HR-XRD analysis results.

	S ₀			S ₁			S ₂		
	2 θ (°)	FWHM(°)	d(Å)	2 θ (°)	FWHM(°)	d(Å)	2 θ (°)	FWHM(°)	d(Å)
(400)	30.17	0.095	2.96	30.34	0.107	2.94	30.54	0.082	2.92
(600)	45.91	0.100	1.97	46.15	0.101	1.96	46.45	0.083	1.95
(12 00)	102.37	0.119	0.99	102.80	0.110	0.98	103.86	0.131	0.97

Ltd, Japan). And then three samples were characterized by HR-XRD (D8 Discover, Bruker, Germany), Room Temperature (RT) Raman scattering and Variable Temperature (VT) Raman scattering spectroscopy (80 K–800 K). The samples were measured by HR-XRD with X-ray wavelength of 1.5406 Å. The 2θ scan with a step of 0.05° is recorded within the angle range of 10°–110°. RT Raman scattering spectroscopy measurements are performed with an excitation laser source of wavelength of 532 nm using a micro-region Raman spectrometer (Finder One, Zolix, China). For VT Raman study between 80 K–800 K we used a temperature-controlled system (T95 System Controllers, Linkam Scientific, UK).

3. Discussion and conclusions

3.1. Energy-dispersive spectroscopy (EDS) and high-resolution X-ray diffraction (HR-XRD)

The results of chemical compositions of Ga, O in sample S₀ and of Ga, Al and O in samples S₁ and S₂ detected by using EDS are displayed in Fig. 1. In EDS study, we have used in all three samples the same e-beam energy 15 KeV and current $\sim 10^{-10}$ A. The EDS measurements showed that the compositions of x (Al) for samples S₁ and S₂ are 9.15%, 20.69%, respectively, which are consistent with the values used in the growth methods.

The microstructures and crystalline phase of three samples are investigated by HR-XRD. The monoclinic Ga₂O₃ (β -Ga₂O₃) belongs to the C_{2/m} space group, with the lattice parameters of $a=12.214$ Å, $b=3.0371$ Å, $c=5.7981$ Å, $\beta=103.83^\circ$. The unit cell of β -Ga₂O₃ consists of two tetrahedrons and two octahedrons among which the tetrahedral Ga atom coordinates with four O atoms, and the octahedral Ga atom coordinates with six O atoms, which are named as [GaO₄] tetrahedron and [GaO₆] octahedron respectively [10, 17]. As shown in Fig. 2 (a), the Al atoms replace the Ga atoms with Al-alloying. The (Al_xGa_{1-x})₂O₃ unit cell volume decreases and the lattice structures distorted, because the Al atom has a smaller radius than that of Ga atom. Fig. 2 (b) presents the HR-XRD spectra of three samples and there are mainly eight diffraction peaks. Referring to the Ga₂O₃ XRD JCPDS card (04-003-1858), these peaks are (200), (400), (600), (800), (-221), (603), (10 00) and (12 00) planes, respectively. It is observed that the diffraction angles increase with the increase of Al content. Among them, the (400), (600) and (12 00) diffraction peaks showed strong signals. The values of three strong XRD peaks and their full width at half maxima (FWHM) are reported in Table 1.

To estimate the lattice distortion, the interplanar crystal spacing can be calculated by the Bragg formula:

$$2d\sin\theta = n\lambda \quad (1)$$

where d is the interplanar crystal spacing, θ is the diffraction angle, λ is the wavelength of X-ray, and n is the diffraction order. Using Equation (1), the interplanar spacings of (400), (600) and (1200) planes for three samples were calculated and the results are shown in Table 1. It can be seen that the interplanar crystal spacing decreases gradually with the increase of Al content. As compared to pure β -Ga₂O₃ the distance of (400) crystal face of (Al_{0.1}Ga_{0.9})₂O₃ decreased by 0.02 Å, and (600) and (1200) interplanar spacing decreased by 0.01 Å, respectively. As for (Al_{0.2}Ga_{0.8})₂O₃ crystal, the distortion of crystal structure became more significant. The interplanar spacing of (400) planes diminished by 0.04 Å, and of (600), (1200) planes decreased by 0.02 Å, respectively.

3.2. RT Raman scattering spectra

The Raman active phonon modes are closely related to the symmetry of the crystal structure. In the monoclinic structure of β -Ga₂O₃ crystal – the two [GaO₆] octahedrons connected with two [GaO₄] tetrahedrons to form double chains along b axis. Each β -Ga₂O₃

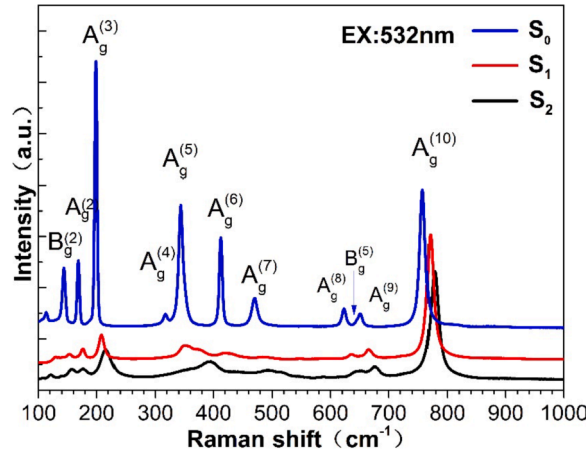


Fig. 3. RT Raman scattering spectra of S_0 , S_1 and S_2 .

Table 2

RT Raman shifts and Raman linewidth of S_0 , S_1 and S_2 .

	S_0		S_1		S_2	
	Raman Shift (cm^{-1})	Raman Linewidth (cm^{-1})	Raman Shift (cm^{-1})	Raman Linewidth (cm^{-1})	Raman Shift (cm^{-1})	Raman Linewidth (cm^{-1})
$B_g^{(2)}$	148.03	5.16	153.36	8.07	158.05	11.81
$A_g^{(2)}$	172.98	3.48	176.25	7.95	179.2	16.69
$A_g^{(3)}$	203.25	3.58	208.45	11.28	217.63	22.67
$A_g^{(4)}$	321.8	5.49				
$A_g^{(5)}$	348.3	9.83	374.92	27.97	393.4	31.88
$A_g^{(6)}$	416.98	5.34	421.92	34.42		
$A_g^{(7)}$	474.6	12.47				
$A_g^{(8)}$	627.86	6.85	635.81	14.28	650.1	23.44
$B_g^{(5)}$	649.12	4.71				
$A_g^{(9)}$	655.47	6.85	665.69	12.77	676.96	18.66
$A_g^{(10)}$	762.27	12.01	770.98	14.58	779.1	18.3

primitive cell consists of 10 atoms, generating 30 phonon modes, 27 of which are the optical phonons. These optical modes at the center of Brillouin zone can be expressed as [18]:

$$\Gamma^{opt} = 10A_g + 5B_g + 4A_u + 8B_u \quad (2)$$

A_g and B_g are symmetrical Raman active phonon modes, while the A_u and B_u are infrared active phonon modes. The Raman active phonon modes of $\beta\text{-Ga}_2\text{O}_3$ can be divided into three parts: 1) the high wavenumber region ($> 600 \text{ cm}^{-1}$), belongs to the stretching and bending of $[\text{GaO}_4]$ tetrahedrons; 2) the medium wavenumber region ($300\text{--}600 \text{ cm}^{-1}$), belongs to the deformation of $[\text{GaO}_4]$ tetrahedrons and $[\text{GaO}_6]$ octahedrons; 3) the low wavenumber region ($< 300 \text{ cm}^{-1}$), belongs to the liberation and translation of the $[\text{GaO}_4]$ chain [3,19,20].

Fig. 3 shows the RT Raman scattering spectra recorded for three samples S_0 , S_1 and S_2 . Clearly the study reveals 11 Raman active modes of $\beta\text{-Ga}_2\text{O}_3$ detected in the frequency range of $100\text{--}1000 \text{ cm}^{-1}$. These modes are assigned as $B_g^{(2)}$, $B_g^{(5)}$, $A_g^{(2)}$, $A_g^{(3)}$, $A_g^{(4)}$, $A_g^{(5)}$, $A_g^{(6)}$, $A_g^{(7)}$, $A_g^{(8)}$, $A_g^{(9)}$, $A_g^{(10)}$, respectively. As compared to the pure $\beta\text{-Ga}_2\text{O}_3$, the Raman peaks of $(\text{Al}_x\text{Ga}_{1-x})_2\text{O}_3$ samples S_1 and S_2 have changed significantly. Except for $A_g^{(10)}$, most of the Raman peaks and their intensities are sharply weakened with FWHMs dramatically broadened. In the Raman spectrum of pure $\beta\text{-Ga}_2\text{O}_3$, the strongest mode is $A_g^{(3)}$. However, in the two $(\text{Al}_x\text{Ga}_{1-x})_2\text{O}_3$ samples S_1 and S_2 – the strongest peak is $A_g^{(10)}$. It is also noticed that the shapes of Raman peaks in the medium wavenumber region become much distorted and are no longer remained as regular Lorentzian shaped peaks. Moreover, their linewidth broadened significantly, which are more than three times larger than those of the pure sample. Obviously, the lattice distortion with Al atoms replacing Ga atoms destroys the symmetry of the crystal structure and weakens the Raman active modes. Moreover, the Al-alloying has a great influence on the Raman modes in the region below $< 700 \text{ cm}^{-1}$, i.e. on the deformation of $[\text{GaO}_4]$ tetrahedrons and $[\text{GaO}_6]$ octahedrons. As the Al atom tends to replace Ga in octahedral sites for $(\text{Al}_x\text{Ga}_{1-x})_2\text{O}_3$ crystals [16], $[\text{GaO}_4]$ tetrahedrons are less distorted than those of $[\text{GaO}_6]$ octahedrons. The vibrational frequencies in high wavenumber region ($> 600 \text{ cm}^{-1}$)

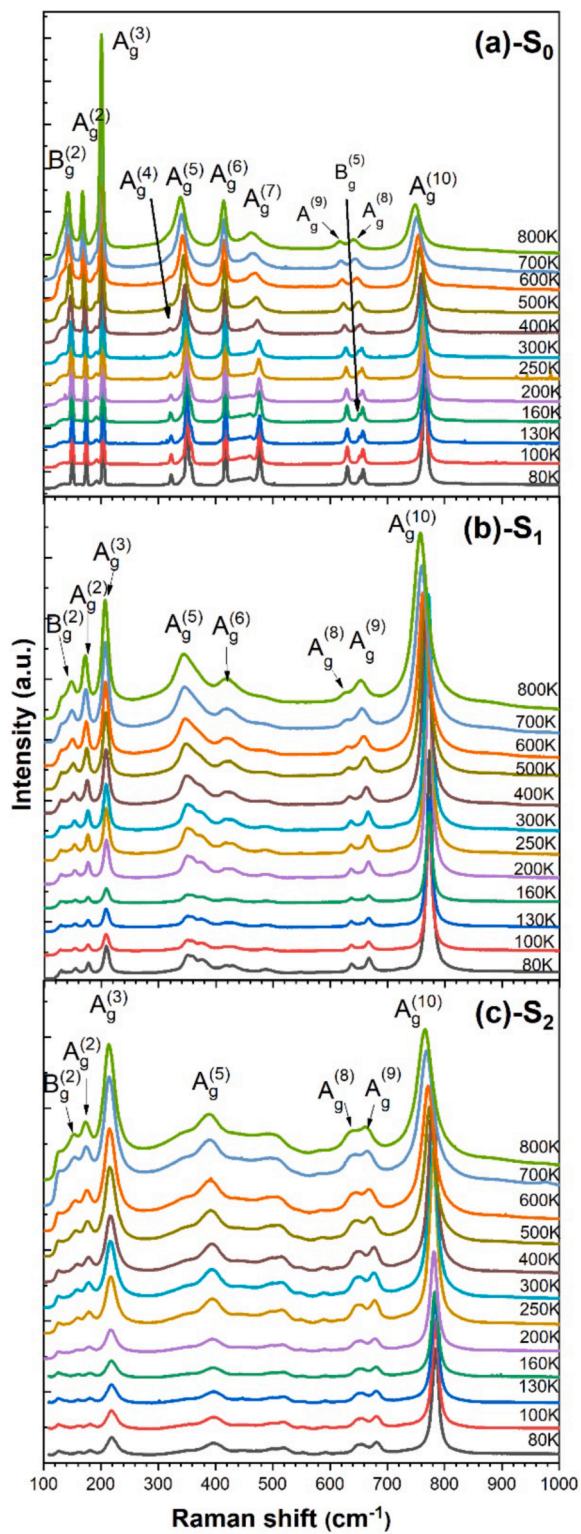


Fig. 4. (a), (b) and (c) are Variable Temperature Raman Spectra of S_0 , S_1 and S_2 in 80 K–800 K, respectively.

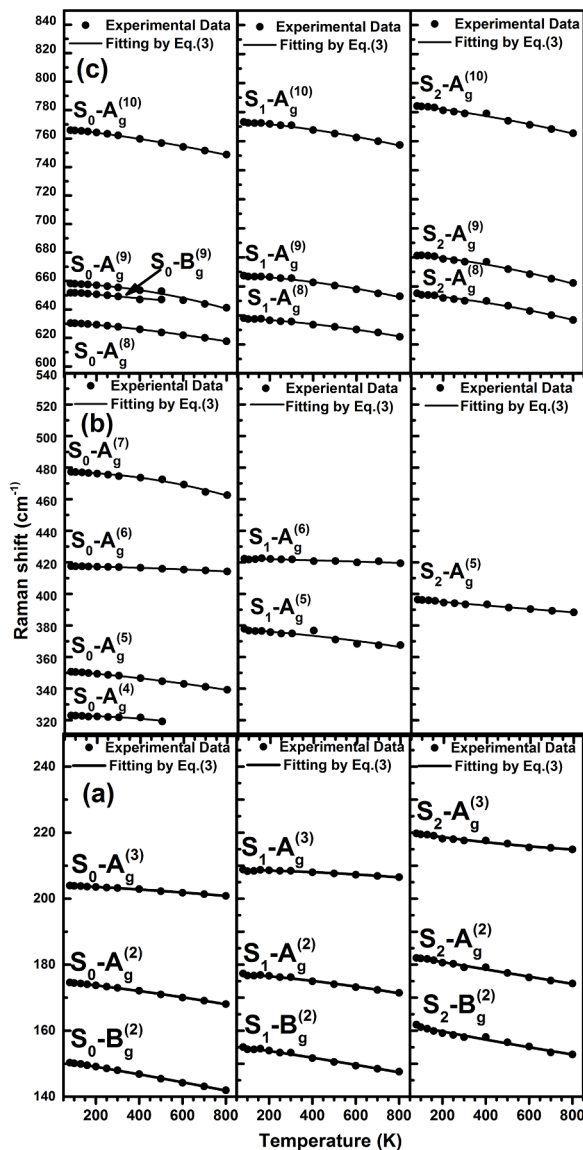


Fig. 5. (a), (b) and (c) are the Raman Shift of S_0 , S_1 and S_2 as a function of temperature, respectively.

which are mainly from $[\text{GaO}_4]$ tetrahedrons are slightly affected, especially for the Raman mode $A_g^{(10)}$. In Table 2 we have reported the RT results of phonon values for all Raman peaks and their FWHMs from the S_0 , S_1 and S_2 samples.

3.3. VT Raman spectra

Fig. 4 (a), (b), (c) are the VT Raman scattering spectra of S_0 , S_1 and S_2 samples. With the increase of temperature, the Raman peaks are redshifted and their FWHMs broadened and peak intensities increased. At higher temperatures, some modes are broadened and overlapped with each other. These modes are $A_g^{(4)}$ and $A_g^{(5)}$, $B_g^{(5)}$ and $A_g^{(9)}$ for the pure sample (S_0), and $A_g^{(8)}$ and $A_g^{(9)}$ modes for the other two $(\text{Al}_x\text{Ga}_{1-x})_2\text{O}_3$ samples (S_1 , S_2). At lower temperatures < 200 K, the intensities of other modes are greatly reduced and almost disappeared (e.g., $B_g^{(2)}$ and $A_g^{(2)}$) for $(\text{Al}_{0.2}\text{Ga}_{0.8})_2\text{O}_3$ sample (S_2). As the temperature increased the lattice vibrations are strengthened and intensities of most Raman modes increased. On the other hand, with the expansion of crystal lattice, the restoring force of the lattice vibration decreased, and the Raman peaks redshifted [21,22]. To some extent, the crystal distortion caused by alloying with Al is restored, and some Raman active modes enhanced (e.g., $A_g^{(6)}$, $A_g^{(9)}$) in S_1 and $A_g^{(5)}$, $A_g^{(8)}$, $A_g^{(9)}$ in S_2 , and all phonon modes in the low wavenumber region, etc.

The temperature dependence of Raman phonon shifts for the three samples displayed in Fig. 4 can be fitted and analyzed by using the following equation [23]:

Table 3
Fitting parameters of the Raman shift vs temperature for S₀, S₁ and S₂, respectively.

	S ₀			S ₁			S ₂		
	$\omega_0(\text{cm}^{-1})$	$\alpha_1 (\times 10^{-3} \text{cm}^{-1}\text{K})$	$\alpha_2 (\times 10^{-6} \text{cm}^{-1}\text{K}^2)$	$\omega_0(\text{cm}^{-1})$	$\alpha_1 (\times 10^{-3} \text{cm}^{-1}\text{K})$	$\alpha_2 (\times 10^{-6} \text{cm}^{-1}\text{K}^2)$	$\omega_0(\text{cm}^{-1})$	$\alpha_1 (\times 10^{-3} \text{cm}^{-1}\text{K})$	$\alpha_2 (\times 10^{-6} \text{cm}^{-1}\text{K}^2)$
$B_g^{(2)}$	151.25	10.60	1.41	155.75	9.20	1.59	162.35	13.28	1.68
$A_g^{(2)}$	175.22	6.92	2.62	177.63	4.82	3.79	183.02	11.19	0.18
$A_g^{(3)}$	204.20	2.84	1.70	208.79	0.84	2.58	220.45	9.77	3.57
$A_g^{(4)}$	322.66	2.74	17.81						
$A_g^{(5)}$	351.65	9.95	7.09	378.14	8.83	7.36	397.34	12.41	1.41
$A_g^{(6)}$	417.75	1.82	3.29	422.60	2.99	9.57			
$A_g^{(7)}$	477.16	0.9	24.50						
$A_g^{(8)}$	631.58	10.35	8.92	638.68	6.87	12.01	655.63	11.2	15.25
$B_g^{(5)}$	653.20	14.41	2.40						
$A_g^{(9)}$	658.60	2.64	24.99	668.11	6.4	16.28	682.69	12.23	17.28
$A_g^{(10)}$	767.5	15.33	10.60	774.22	10.02	14.46	785.72	16.92	10.85

$$\omega = \omega_0 - \alpha_1 T - \alpha_2 T^2 \quad (3)$$

where ω_0 is the Raman shift when temperature is 0 K, α_1 and α_2 are the first- and second-order temperature coefficients, respectively.

The results are shown in Fig. 5, in which the solid lines are the fitting curves using Eq. (3), with parameter values of ω_0 , α_1 and α_2 are recorded in Table 3. Clearly all modes and their Raman shifts as a function of temperature are well represented by Eq. (3). The decrease of Raman shifts of optical phonons with increasing temperature is mainly due to change of harmonic frequency with volume expansion and the anharmonic coupling to phonons of other branches. The lattice distortion and change of crystal symmetry affected both α_1 and α_2 parameters. It is noteworthy that almost each mode of (Al_{0.2}Ga_{0.8})₂O₃ has the largest α_1 . The features of α_1 and α_2 in Table 3 indicate that the Al-alloying induced complex lattice vibrations and phonon coupling.

The temperature-dependent linewidth of each Raman active mode are presented in Fig. 6 of the three samples. In Fig. 6, as seen intuitively, the FWHMs of Raman peaks are enhanced with the increase of temperature and Al content. In the low wavenumber region and with the increase of Al component (x) from 0 to 20%, the linewidths of $B_g^{(2)}$, $A_g^{(2)}$, and $A_g^{(3)}$ modes broadened $\sim 3 \text{ cm}^{-1}$ and 9 cm^{-1} , 3 cm^{-1} and 9 cm^{-1} , and 8 cm^{-1} and 19 cm^{-1} at RT, respectively. In particular, the linewidths of modes of S₂ sample increase sharply. With the increase of temperature, the linewidths of all Raman active phonons of S₀; $A_g^{(2)}$, $A_g^{(3)}$, $A_g^{(9)}$, $A_g^{(10)}$ modes of S₁; and $A_g^{(3)}$, $A_g^{(5)}$, $A_g^{(8)}$, $A_g^{(9)}$, $A_g^{(10)}$ modes of S₂, are widened monotonically. However, the linewidths of $B_g^{(2)}$ and $A_g^{(8)}$ from S₁ sample first broadened and then became narrower. Different from the other modes, the linewidths of $A_g^{(5)}$, $A_g^{(6)}$ from S₁, and $A_g^{(2)}$, $B_g^{(2)}$ from S₂, displayed irregular variations. Usually, the broadening of Raman bands mainly caused by anharmonicity phenomena can be expressed by the following cubic and quartic terms [19]:

$$\Gamma = A \left[\left(e^{\hbar\omega_0/2k_B T} - 1 \right)^{-1} + \frac{1}{2} \right] + B \left\{ \left[\left(e^{\hbar\omega_0/3k_B T} - 1 \right)^{-1} + \frac{1}{2} \right]^2 + \frac{1}{12} \right\} \quad (5)$$

where k_B is Boltzmann's constant, A and B are two constants. The cubic term describes the destruction of one phonon of ω_0 frequency into two phonons which equal to $\omega_0/2$. And the quartic term can be associated with the destruction of one phonon of $\omega_0/3$ frequency [19,24]. In Fig. 5, except for $A_g^{(2)}$, $A_g^{(3)}$, the linewidths changing with temperature of most Raman modes of pure β -Ga₂O₃, can be fitted well by above expression (5), especially for those modes in the medium and high wavenumber regions (see the solid lines in Fig. 5). But for almost all of Raman modes of two Al-alloyed β -Ga₂O₃ crystals, the Raman linewidths cannot be fitted by formula (5). The results indicate that the deformation of lattice structure of Al-alloyed β -Ga₂O₃ has complicated changes with the increase of temperature, and more causes contribute to the broadening properties of Raman bands.

4. Conclusion

In summary, we have reported the results of microcrystalline structure and phonon characteristics of three single crystals β -Ga₂O₃, (Al_{0.1}Ga_{0.9})₂O₃ and (Al_{0.2}Ga_{0.8})₂O₃ grown by EFG and OFZ methods. The lattice structures are found distorted with Al-alloying. The HR-XRD results revealed values of interplanar crystal spacing decreasing with the increase of Al contents. As compared to the pure β -Ga₂O₃, the interplanar spacing of (400), (600) and (12 00) decreased by 0.02 Å, 0.01 Å and 0.01 Å, respectively for (Al_{0.1}Ga_{0.9})₂O₃ and shrunk by 0.04 Å, 0.02 Å and 0.02 Å, respectively for (Al_{0.2}Ga_{0.8})₂O₃. The Raman scattering measurements have found Raman active modes redshifted and their FWHMs widened with Al-alloying. The Raman active modes in the medium and low wavenumber regions ($< 600 \text{ cm}^{-1}$) were greatly weakened, indicating that the Al-doping mainly affected the deformation of [GaO₄] tetrahedrons

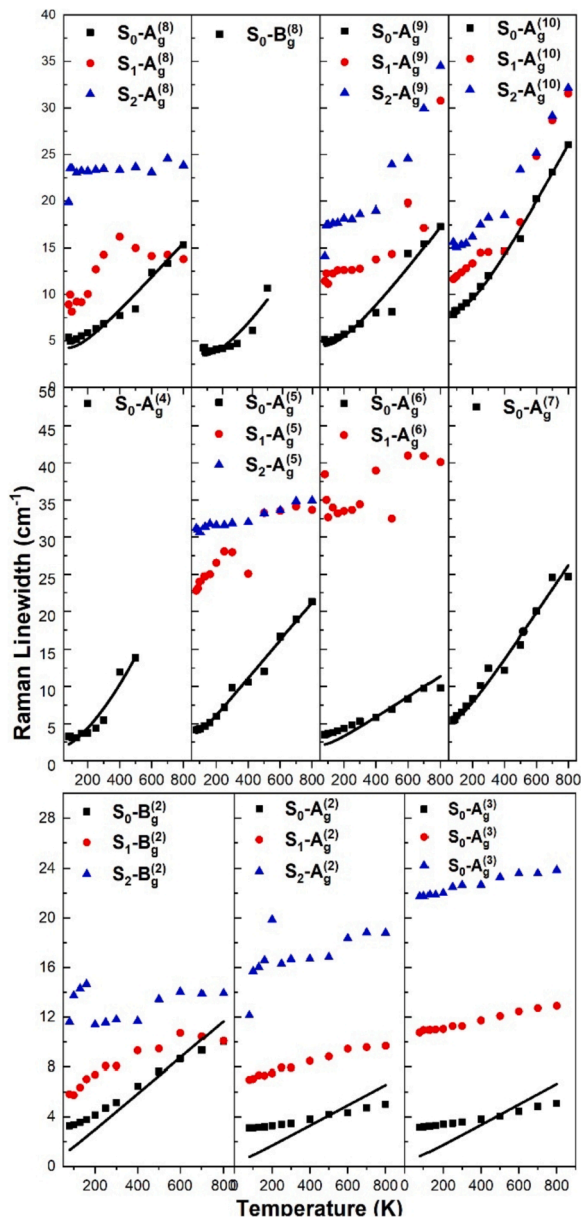


Fig. 6. Temperature dependence of the Raman linewidths of S_0 , S_1 and S_2 , respectively (Solid lines are fitting by formula (5)).

and $[\text{GaO}_6]$ octahedrons, and the liberation and translation of the $[\text{GaO}_4]$ chain. With the increase of temperature, the Raman peaks are also redshifted and their FWHMs broadened. For the $\text{Al}_x\text{Ga}_{1-x}\text{O}_3$ samples, some Raman modes are broadened and merged at high temperatures, while the others are weakened and disappeared at low temperatures. By numerical fitting, the specific relationships between the Raman shifts and temperatures are determined, and the broadening properties of each Raman mode dependent on Al content and temperature were analyzed. This work has clearly provided significant results of microstructures and phonon features for understanding the basic characteristics of $\text{Al}_x\text{Ga}_{1-x}\text{O}_3$ and their potential use in device applications.

Authors' statement

In this study, Lingyu Wan and Xian Chen proposed the study and drafted the manuscript; Huiyuan Cui and Changtai Xia prepared the samples; Xian Chen and Wenlong Niu did measuring experiments and discussed data with Lingyu Wan; Zhe Chuan Feng, Devki N. Talwar and Changtai Xia provided a lot of advice and guidance for English improvement. All authors gave final approval for this submission and agreed to be held accountable for the work performed therein.

Declaration of competing interest

We declare that there is no commercial or related conflict of interest between the authors of this paper submission.

Acknowledgements

This work was supported by the National Natural Science Foundation of China [Nos. 61367004 and 51972319], the Guangxi Natural Science Foundation (No. 2017JJA170740y), and the project supported by State Key Laboratory of Luminescence and Applications (No. SKLA-2019-06).

References

- [1] S. Rafique, L. Han, M.J. Tadjer, J.A.F. Jr, N.A. Mahadik, H. Zhao, Homoepitaxial growth of β -Ga₂O₃ thin films by low pressure chemical vapor deposition, *Appl. Phys. Lett.* 108 (2016) 182105, <https://doi.org/10.1063/1.4948944>.
- [2] Z.Z. Hu, Q. Feng, J.C. Zhang, F.G. Li, X. Li, Z.Q. Feng, C.F. Zhang, Y. Hao, Optical properties of (Al_xGa_{1-x})₂O₃ on sapphire, *Superlattice. Microst.* 114 (2018) 82–88, <https://doi.org/10.1016/j.spmi.2017.12.013>.
- [3] J. Yoo, S. Rafique, A. Lange, H.P. Zhao, S. Elhadji, Lifetime laser damage performance of β -Ga₂O₃ for high power applications, *Apl. Mater.* 6 (2018), 036105, <https://doi.org/10.1063/1.5021603>.
- [4] S.H. Yuan, S.L. Ou, C.M. Chen, S.Y. Huang, B.W. Hsiao, D.S. Wu, Characterization of aluminum gallium oxide films grown by pulsed laser deposition, *Ceram. Int.* 45 (2019) 702–707, <https://doi.org/10.1016/j.ceramint.2018.09.232>.
- [5] M. Hilfiker, U. Kilic, A. Mock, V. Darakchieva, S. Knight, R. Korlacki, A. Mauze, Y. Zhang, J. Speck, M. Schubert, Dielectric function tensor (1.5 eV to 9.0 eV), anisotropy, and band to band transitions of monoclinic β -(Al_xGa_{1-x})₂O₃ (x<0.21) films, *Appl. Phys. Lett.* 114 (2019) 231901, <https://doi.org/10.1063/1.5097780>.
- [6] C.C. Wang, S.H. Yuan, S.L. Ou, S.Y. Huang, K.Y. Lin, Y.A. Chen, P.W. Hsiao, D.S. Wu, Growth and characterization of co-sputtered aluminum-gallium oxide thin films on sapphire substrates, *J. Alloys Compd.* 765 (2018) 894–900, <https://doi.org/10.1016/j.jallcom.2018.06.270>.
- [7] M. Baldini, M. Albrecht, D. Gogova, R. Schewski, G. Wagner, Effect of indium as a surfactant in (Ga_{1-x}In_x)₂O₃ epitaxial growth on β -Ga₂O₃ by metal organic vapour phase epitaxy, *Semicond. Sci. Technol.* 30 (2015), 024013, <https://doi.org/10.1088/0268-1242/30/2/024013>.
- [8] Y.S. Rim, H.W. Choi, K.H. Kim, H.J. Kim, H.J. K, Effects of structural modification via high-pressure annealing on solution-processed InGaO films and thin-film transistors, *J. Phys. D Appl. Phys.* 49 (2016), 075112, <https://doi.org/10.1088/0022-3727/49/7/075112>.
- [9] Y.W. Zhang, Z.B. Xia, J. Mcglone, W.Y. Sun, C. Joishi, A.R. Arehart, S.A. Ringel, S. Rajan, Evaluation of low-temperature saturation velocity in β -(Al_xGa_{1-x})₂O₃/Ga₂O₃ modulation-doped field-effect transistors, *IEEE Trans. Electron. Dev.* 66 (2019) 1574–1578, <https://doi.org/10.1109/TED.2018.2889573>.
- [10] J. Wang, L.J. Ye, X. Wang, H. Zhang, L. Li, C.Y. Kong, W.J. Li, High transmittance β -Ga₂O₃ thin films deposited by magnetron sputtering and post-annealing for solar-blind ultraviolet photodetector, *J. Alloys Compd.* 803 (2019) 9–15, <https://doi.org/10.1016/j.jallcom.2019.06.224>.
- [11] B.W. Krueger, C.S. Dandeneau, E.M. Nelson, S.T. Dunham, F.S. Ohuchi, M.A. Olmstead, Variation of band gap and lattice parameters of β -(Al_xGa_{1-x})₂O₃ powder produced by solution combustion synthesis, *J. Am. Ceram. Soc.* 99 (2016) 2467–2473, <https://doi.org/10.1111/jace.14222>.
- [12] V.S. Escrivano, J.M.G. Amores, E.F. Lopez, M. Panizza, C. Resini, G. Busca, Solid state characterization of coprecipitated alumina-gallia mixed oxide powders, *J. Mater. Sci.* 40 (2005) 2013–2021, <https://doi.org/10.1007/s10853-005-1225-3>.
- [13] J. Li, X.H. Chen, T.C. Ma, X.Y. Cui, F.F. Ren, S.L. Gu, R. Zhang, Y.D. Zheng, S.P. Ringer, L. Fu, H.H. Tan, C. Jagadish, J.D. Ye, Identification and modulation of electronic band structures of single-phase β -(Al_xGa_{1-x})₂O₃ alloys grown by laser molecular beam epitaxy, *Appl. Phys. Lett.* 113 (2018), 041901, <https://doi.org/10.1063/1.5027763>.
- [14] C. Kranert, M. Jenderka, J. Lenzner, M. Lorenz, H.V. Wemckstern, R. Schmidt-grund, M. Grundmann, Lattice parameters and Raman-active phonon modes of β -(Al_xGa_{1-x})₂O₃, *J. Appl. Phys.* 117 (2015) 125703, <https://doi.org/10.1063/1.4915627>.
- [15] X.F. Ma, Y.M. Zhang, L.P. Dong, R.X. Jia, First-principles calculations of electronic and optical properties of aluminum-doped β -Ga₂O₃ with intrinsic defects, *Results Phys* 7 (2017) 1582–1589, <https://doi.org/10.1016/j.rinp.2017.04.023>.
- [16] H.L. Xiao, G.Q. Shao, Q.L. Sai, C.T. Xia, S.M. Zhou, X.Z. Yi, Wide bandgap engineering of β -(Al,Ga)₂O₃ mixed crystals, *J. Inorg. Mater.* 31 (2016) 1258–1262, <https://doi.org/10.15541/jim20160135>.
- [17] Q. Cao, L.N. He, H.D. Xiao, X.J. Feng, Y.J. Lv, J. Ma, β -Ga₂O₃ epitaxial films deposited on epi-GaN/sapphire (0001) substrates by MOCVD, *Mater. Sci. Semicond. Process.* 77 (2018) 58–63, <https://doi.org/10.1016/j.mssp.2018.01.010>.
- [18] C. Kranert, C. Sturm, R. Schmidt-grund, M. Grundmann, Raman tensor elements of β -Ga₂O₃, *Nat. Publ. Gr.* (2016) 1–9, <https://doi.org/10.1038/srep35964>.
- [19] T. Sakurai, T. Sato, Temperature dependence of vibrational spectra in calcite by means of emissivity measurement, *Phys. Rev. B* 4 (1971) 583–591, <https://doi.org/10.1103/physrevb.4.583>.
- [20] C. Vigreux, L. Binet, D. Gourier, Formation by laser impact of conducting β -Ga₂O₃-in₂O₃ solid solutions with composition gradients, *J. Solid State Chem.* 157 (2001) 94–101, <https://doi.org/10.1006/jssc.2000.9043>.
- [21] G. Irmer, J. Monecke, The temperature dependence of the LO (Γ) and TO (Γ) phonons in GaAs and InP, *phys. stat. sol* (1996) 85–95, <https://doi.org/10.1002/psb.222195010> (b) 195.
- [22] J. Menendez, M. Cardona, Temperature dependence of the first-order Raman scattering by phonons in Si, Ge, and α -Sn: anharmonic effects, *Phys. Rev. B* 29 (1984) 2051–2059, <https://doi.org/10.1103/physrevb.29.2051>.
- [23] W.S. Li, Z.X. Shen, Z.C. Feng, S.J. Chua, Temperature dependence of Raman scattering in hexagonal gallium nitride films, *J. Appl. Phys.* 87 (2011) 333 2–3337, <https://doi.org/10.1063/1.3594697>.
- [24] D. Dohy, G. Lucazeau, A. Revcolevschi, Raman spectra and valence force field of single-crystalline β -Ga₂O₃, *J. Solid State Chem.* 45 (1982) 180–192, [https://doi.org/10.1016/0022-4596\(82\)90274-2](https://doi.org/10.1016/0022-4596(82)90274-2).